

Diffraction-focusing migration velocity analysis

Paul Sava and Biondo Biondi, Stanford University
John Etgen, BP E&P Technology Group

SUMMARY

We propose a method for estimating interval velocity using kinematic information in diffractions. We extract velocity information after migration by analyzing residual diffraction focusing in physical space using prestack residual migration. We invert for interval velocity using a wavefield-continuation operator linking velocity perturbations to perturbations of migrated images. We measure the accuracy of the migration velocity using a diffraction-focusing criterion, instead of the criterion of flatness of migrated common-image gathers that is commonly employed in Migration Velocity Analysis (MVA). This criterion enables us to extract velocity information from events that would be challenging to use with conventional MVA methods, and thus it makes our method a powerful complement to conventional MVA.

INTRODUCTION

Migration velocity analysis (MVA) using diffracted events is not a new concept. Harlan (1986) proposes methods to isolate diffraction events around faults using statistical tools, and introduces MVA techniques applicable to simple geology, e.g. constant velocity or $v(z)$. Similarly, de Vries and Berkhout (1984) use the concept of minimum entropy to evaluate diffraction focusing and apply this methodology to MVA. Soellner and Yang (2002) use focusing of diffractions simulated using data-derived parameters to estimate interval velocities. Khaidukov et al. (2004) propose methods to isolate diffracted energy from the seismic data which can be used as velocity analysis indicators.

Sava and Biondi (2004a,b) introduce a method of wave-equation migration velocity analysis (WEMVA), which finds a slowness perturbation corresponding to an image perturbation. This methodology is similar to ray-based migration tomography (Al-Yahya, 1989; Stork, 1992; Etgen, 1993), where the slowness perturbation is derived from depth errors, and to wave-equation tomography (Tarrantola, 1986; Woodward, 1992; Pratt, 1999) where the slowness perturbation is derived from measured wavefield perturbations.

The moveout information given by the specular energy is not the only information contained by an image migrated with an incorrect slowness. Non-specular diffracted energy is present in the image and indicates slowness inaccuracies. Traveltime-based MVA methods cannot easily deal with the diffraction energy, and are mostly concerned with moveout analysis. In contrast, a difference between an inaccurate image and a perfectly focused target image contains both specular and non-specular energy; therefore WEMVA is naturally able to derive velocity updates based on both these types of information.

One possible application of this technique in seismic imaging concerns areas with abundant, clearly identifiable diffractions. Examples include highly fractured reservoirs, carbonate reservoirs, rough salt bodies and reservoirs with complicated stratigraphic features. Of particular interest is the case of salt bodies. Diffractions can help estimate more accurate velocities at the top of the salt, particularly in the cases of rough salt bodies. Moreover, diffraction energy may be the most sensitive velocity information we have from under the salt, since most of the reflected energy we record at the surface has only a narrow range of angles of incidence at the reflector, rendering the analysis of moveout ambiguous.

WEMVA THEORY

Imaging by wavefield extrapolation (WE) is based on recursive

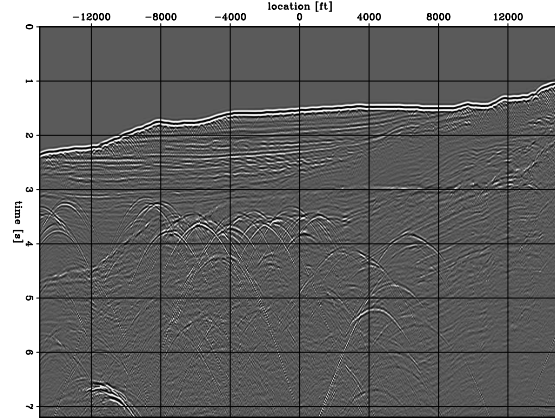


Figure 1: Zero-offset synthetic data used for focusing migration velocity analysis.

continuation of the wavefields (\mathcal{U}) using an extrapolation operator (\mathbf{E}):

$$\mathcal{U}_{z+\Delta z} = \mathbf{E}_z [\mathcal{U}_z] . \quad (1)$$

At any depth z , the wavefield ($\tilde{\mathcal{U}}$), extrapolated through the background medium characterized by the background velocity (\bar{s}), interacts with medium perturbations (Δs) and creates wavefield perturbations ($\Delta \mathcal{V}$):

$$\Delta \mathcal{V}_z = \mathbf{S}_z (\tilde{\mathcal{U}}_z) [\Delta s_z] . \quad (2)$$

\mathbf{S} is a scattering operator relating slowness perturbations to wavefield perturbations. The total wavefield perturbation at depth $z + \Delta z$ is the sum of the perturbation accumulated up to depth z from all depths above ($\Delta \mathcal{U}_z$), plus the scattered wavefield from depth ($\Delta \mathcal{V}_z$) extrapolated one depth step (Δz):

$$\Delta \mathcal{U}_{z+\Delta z} = \mathbf{E}_z [\Delta \mathcal{U}_z] + \mathbf{E}_z [\mathbf{S}_z (\tilde{\mathcal{U}}_z) [\Delta s_z]] . \quad (3)$$

We can use the recursive equation (3) to compute a wavefield perturbation, given a precomputed background wavefield and a slowness perturbation. From the wavefield perturbation ($\Delta \mathcal{U}$), we can compute an image perturbation ($\Delta \mathcal{R}$) by applying an imaging condition, $\Delta \mathcal{R} = \mathbf{I} \Delta \mathcal{U}$. If we accumulate all scattering, extrapolation and imaging into a single operator we can write a linear expression relating an image perturbation ($\Delta \mathcal{R}$) to a slowness perturbation (Δs):

$$\Delta \mathcal{R} = \mathbf{L} \Delta s . \quad (4)$$

For wave-equation migration velocity analysis, we use equation (4) to estimate a perturbation of the slowness model from a perturbation of the migrated image by minimizing the objective function

$$J(\Delta s) = \|\mathbf{W}(\Delta \mathcal{R} - \mathbf{L} \Delta s)\|^2 + \epsilon^2 \|\mathbf{A} \Delta s\|^2 . \quad (5)$$

\mathbf{A} can be a regularization operator which penalizes rough features of the model, \mathbf{W} is a weighting operator related to the inverse of the data covariance, indicating the reliability of the data residuals, and ϵ is a scalar parameter which balances the relative importance of the data residual, $\mathbf{W}(\Delta \mathcal{R} - \mathbf{L} \Delta s)$, and the model residual, $(\mathbf{A} \Delta s)$.

Diffraction-focusing MVA

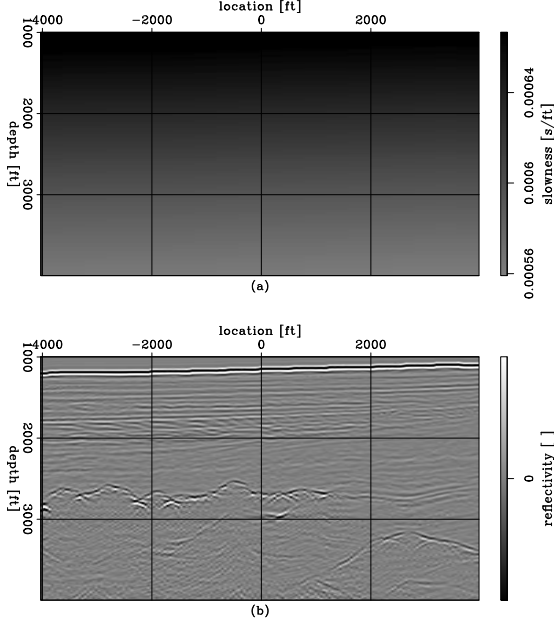


Figure 2: Zero-offset migrated image for the synthetic data in Figure 1: velocity model (a), and migrated image (b). Migration using the initial $v(z)$ velocity model.

An essential element of our velocity analysis method is the image perturbation, $\Delta\mathcal{R}$. For the purposes of the optimization problem in equation (5), this object is known and has to be precomputed, together with the background wavefield used by the operator \mathbf{L} .

A simple way to define the image perturbation ($\Delta\mathcal{R}$) is to take the image obtained with the background slowness and improve it by applying an image enhancement operator. In principle, both focusing in space (along the midpoint axis) and focusing in offset are velocity indicators, and they should be used together to achieve the highest accuracy. Here, we emphasize migration velocity analysis using only focusing of diffractions along the spatial axes.

We use prestack Stolt residual migration (Stolt, 1996; Sava, 2003) as the image enhancement operator (\mathbf{K}). This residual migration operator applied to the background image creates new images (\mathcal{R}), functions of a scalar parameter (ρ), which represents the ratio of a new slowness model relative to the background one:

$$\mathcal{R} = \mathbf{K}(\rho)[\mathcal{R}_b]. \quad (6)$$

We can now take the image perturbation to be the difference between the *improved* image (\mathcal{R}) and the *background* image (\mathcal{R}_b): $\Delta\mathcal{R} = \mathcal{R} - \mathcal{R}_b$. The challenge with this method of constructing image perturbations for WEMVA is that the two images, \mathcal{R} and \mathcal{R}_b , can get out of phase, such that they risk violating the requirements of the first-order Born approximation (Sava and Biondi, 2004a).

We address this challenge by using *linearized image perturbations*. We run residual migration for a large number of parameters ρ and pick at every location the value where the image is best focused. Then we estimate at every point the gradient of the image relative to the ρ parameter and construct the image perturbations using the following relation:

$$\Delta\mathcal{R} \approx \mathbf{K}' \Big|_{\rho=1} [\mathcal{R}_b] \Delta\rho, \quad (7)$$

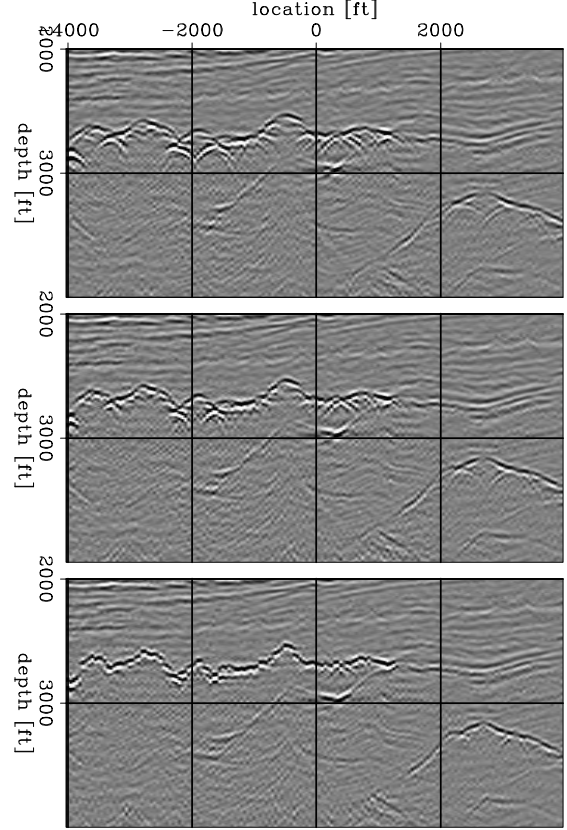


Figure 3: Residual migration applied to the image migrated with the initial velocity model, Figure 2. From top to bottom, the images correspond to the ratios $\rho = 1.04, 1.00, 0.96, 0.92, 0.88$.

where, by definition, $\Delta\rho = 1 - \rho$. The main benefit of constructing image perturbations with equation (7) is that we avoid the danger of subtracting images that are out of phase.

EXAMPLE

We test our methodology using a synthetic dataset obtained by acoustic finite-difference modeling over a salt body. Although we use our technique to constrain the top of the salt, the methodology is applicable in any situation where diffractions are available, for example, subsalt where angular coverage is small, and uncollapsed diffractions carry substantial information which is disregarded in typical MVA methodologies.

Figure 1 shows the zero-offset data we use for velocity analysis to delineate the top of the rough salt body. The section contains a large number of diffractors, whose focusing allows us to constrain the overburden velocity model.

Figure 2(a) depicts the starting velocity model, and Figure 2(b) depicts the initial image obtained by zero-offset migration. The starting velocity is a typical Gulf of Mexico $v(z)$ function hanging from the water bottom. Uncollapsed diffractions are visible at the top of the salt, indicating that the velocity in the overburden is not accurate. Such defocusing also hampers our ability to pick accurately the top of the salt and, therefore, degrades imaging at depth.

We run residual migration on the background image (Figure 2). Figure ?? shows this image after residual migration with various velocity ratios (Sava, 2003). From top to bottom, the ratios are:

Diffraction-focusing MVA

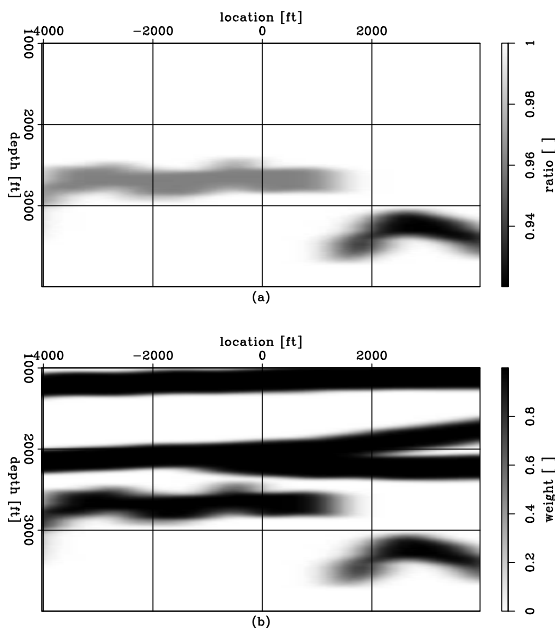


Figure 4: Residual migration picks (a) and the associated confidence weights (b).

1.04, 1.00, 0.96, 0.92, 0.88. Different parts of the image come into focus at different values of the velocity ratio.

Figure 4(a) shows the picked velocity ratios at various locations in the image. The white background corresponds to picked $\Delta\rho = 0$, and the gray shades correspond to $\Delta\rho$ between 0 and 0.08. Figure 4(b) shows a map of the weights (\mathbf{W}) associated to each picked value. The white background corresponds to $\mathbf{W} = 0$, indicating low confidence in the picked values, and the dark regions correspond to $\mathbf{W} = 1$, indicating high confidence in the picked values.

Figure 5(a) shows the slowness perturbation obtained after 20 iterations of inversion from the image perturbation in Figure 5(b). The smooth slowness perturbation is constrained by a regularization operator (Laplacian). Figure 6(a) shows the updated slowness model and Figure 6(b) shows the zero-offset migrated image corresponding to the updated model. Most of the diffractions at the top of the salt have been collapsed, and the rough top of the salt can be easily picked. The diffractions corresponding to the salt bodies at $x = 2000 - 4000$ ft, $z = 3500$ ft are not fully collapsed, indicating that another nonlinear iteration involving residual migration and picking is necessary.

Finally, Figure 7 shows prestack migrated images using the initial velocity model (a) and the one updated using zero-offset focusing (b). The top panels depict stacks, and the bottom panels depict angle-domain common-image gathers (ADCIG) (Sava and Fomel, 2003). The ADCIGs show substantial bending after migration with the initial velocity, but they are mostly flat after migration with the updated velocity, although none of the moveout information has been used for velocity update. Figure 8 shows two ADCIGs at $x = -2350$ ft from the images obtained with the initial velocity model (a) and the updated velocity model (b). The ADCIG in panel (a) corresponds to a notch in the top of the salt and is complicated to use for velocity analysis. However, after migration with the updated velocity model, panel (b), the ADCIG is much simpler, and the small residual moveouts can be picked for velocity updates.

A comparison of Figure 6(b) with Figure 7(b) shows a potential

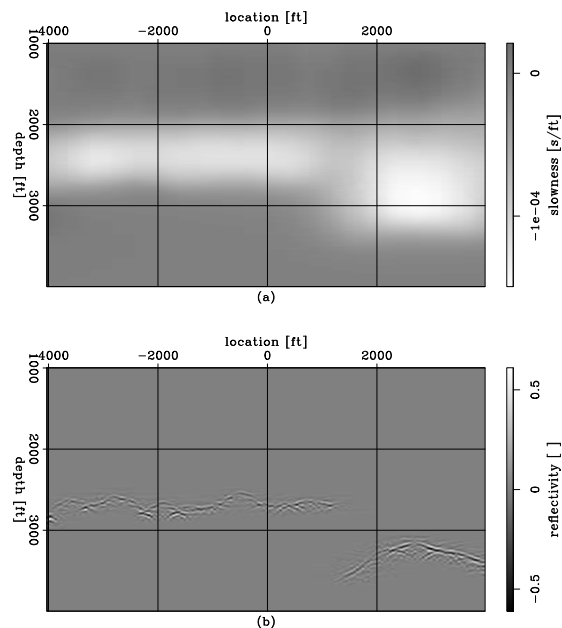


Figure 5: Slowness perturbation (a), derived from an image perturbation (b) derived from the background image in Figure 2 and the velocity ratio picks in Figure 4.

limitation of our technique in the presence of prismatic waves (Biondi, 2003). Both images are obtained with the same velocity, the first one with zero-offset data and the second one with prestack data. The imaging artifacts visible at the bottom of the deep canyons at the top of the salt in Figure 6(b) are created by prismatic waves that are not properly imaged from zero-offset data. Prismatic waves are better (though not perfectly) handled by full prestack migration, and thus the artifacts are not visible in the prestack-migrated image shown in Figure 7(b). Since these artifacts resemble uncollapsed diffractions, they may mislead the analysis of the residual migrated images and be interpreted as symptoms of velocity inaccuracies.

CONCLUSIONS

Diffractions contain velocity information that is overlooked by conventional MVA methods, which use flatness of common image gathers as the only criterion for the accuracy of migration velocity. We demonstrate that accurate interval-velocity can be estimated by inverting the results of a residual-focusing analysis of migrated diffracted events. To convert residual-focusing measurements into interval-velocity updates, we employ the WEMVA methodology which is ideally suited for this task because it inverts image perturbations directly, without requiring an estimate of the reflector geometry.

Our example demonstrates how the proposed method can exploit the velocity information contained in the event generated by a rugose salt-sediment interface. This kind of events is present in many salt-related data sets, and the ability of using the diffracted energy to further constrain the velocity model might significantly improve the final imaging results.

ACKNOWLEDGMENTS

We would like to acknowledge the financial support of the sponsors of the Stanford Exploration Project (SEP), and Frederic Billeter (BP) for providing the synthetic salt-dome dataset.

Diffraction-focusing MVA

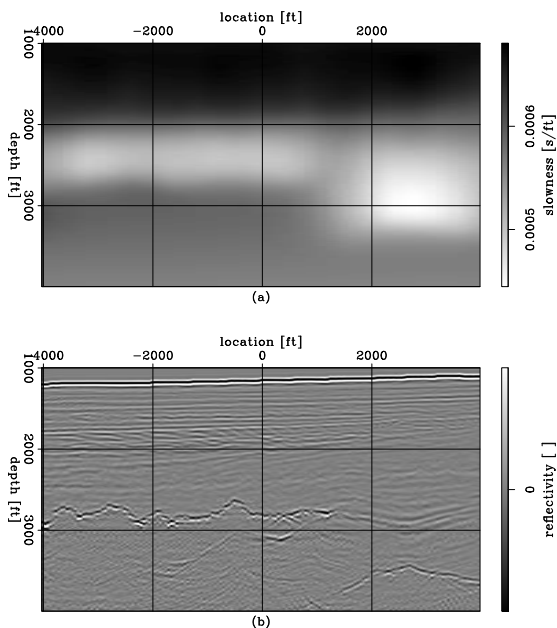


Figure 6: Zero-offset migrated image for the synthetic data in Figure 1: velocity model (a), and migrated image (b). Migration using the updated velocity.

REFERENCES

Al-Yahya, K. M., 1989, Velocity analysis by iterative profile migration: *Geophysics*, **54**, 718–729.

Biondi, B. L., 2003, 3-D Seismic Imaging: <http://sepwww.stanford.edu/sep/biondi/Lectures/index.html>.

Etgen, J. T., 1993, Interval velocity estimation using residual prestack migration in 63rd Ann. Internat. Mtg. Soc. of Expl. Geophys., 669–672.

Harlan, W. S., 1986, Signal-noise separation and seismic inversion: Ph.D. thesis, Stanford University. URL <http://sepwww.stanford.edu/oldreports/sep47/index.html>.

Khaidukov, V., Landa, E., and Moser, T., 2004, Diffraction imaging by focusing-defocusing: an outlook on seismic superresolution: *Geophysics*, submitted for publication.

Pratt, R. G., 1999, Seismic waveform inversion in the frequency domain, Part 1: Theory and verification in a physical scale model: *Geophysics*, **64**, 888–901.

Sava, P., 2003, Prestack residual migration in the frequency domain: *Geophysics*, **67**, 634–640.

Sava, P., and Biondi, B., 2004a, Wave-equation migration velocity analysis—I: Theory: *Geophysical Prospecting*, submitted for publication.

—, 2004b, Wave-equation migration velocity analysis—II: Examples: *Geophysical Prospecting*, submitted for publication.

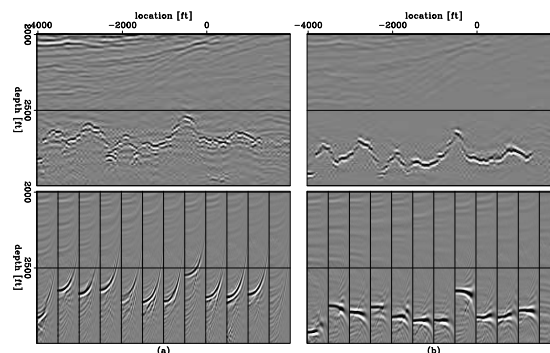


Figure 7: Prestack migrated images using the initial velocity model (a) and the updated velocity model (b). The top panels depict image stacks and the bottom panels depict angle-domain common image gathers.

Sava, P., and Fomel, S., 2003, Angle-domain common image gathers by wavefield continuation methods: *Geophysics*, **68**, 1065–1074.

Soellner, W., and Yang, W., 2002, Diffraction response simulation: A 3D velocity inversion tool in 72nd Ann. Internat. Mtg. Soc. of Expl. Geophys., 2293–2296.

Stolt, R. H., 1996, Short note - A prestack residual time migration operator: *Geophysics*, **61**, 605–607.

Stork, C., 1992, Reflection tomography in the postmigrated domain: *Geophysics*, **57**, 680–692.

Tarantola, A., 1986, A strategy for nonlinear elastic inversion of seismic reflection data: *Geophysics*, **51**, 1893–1903.

de Vries, D., and Berkhout, A. J., 1984, Velocity analysis based on minimum entropy: *Geophysics*, **49**, 2132–2142.

Woodward, M. J., 1992, Wave-equation tomography: *Geophysics*, **57**, 15–26.

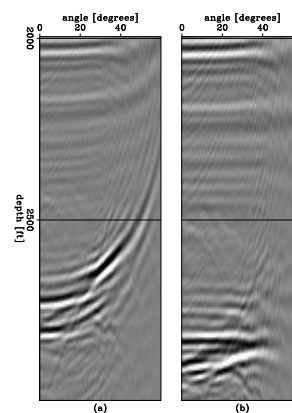


Figure 8: Angle-domain common image gather obtained after migration with the initial velocity model (a) and the updated velocity model (b).